ARMY RESEARCH LABORATORY

Improvements to the Processing and Characterization of Needled Composite Laminates

by Ryan Emerson, Bradley Lawrence, Andrew Montgomery, and Sirina Safriet

ARL-RP-472 **January 2014**

A reprint from the *Proceedings of the American Society for Composites 28th Technical Conference*, State College, PA, September 2013.

NOTICES

Disclaimers

The findings in this report are not to be construed as an official Department of the Army position unless so designated by other authorized documents.

Citation of manufacturer's or trade names does not constitute an official endorsement or approval of the use thereof.

Destroy this report when it is no longer needed. Do not return it to the originator.

Army Research Laboratory
Aberdeen Proving Ground, MD 21005-5069

ARL-RP-472 **January 2014**

Improvements to the Processing and Characterization of Needled Composite Laminates

Ryan Emerson
Weapons and Materials Research Directorate, ARL

Bradley Lawrence
Bowhead Science and Technology

Andrew Montgomery
Science and Mathematics Academy

Sirina Safriet
Material and Manufacturing Directorate

A reprint from the *Proceedings of the American Society for Composites 28th Technical Conference*, State College, PA, September 2013.

REPORT DOCUMENTATION PAGE

Form Approved
OMB No. 0704-0188

1. REPORT DATE *(DD-MM-YYYY)*	2. REPORT TYPE	3. DATES COVERED (From - To)
January 2014	Reprint	January 2012–August 2013

4. TITLE AND SUBTITLE
Improvements to the Processing and Characterization of Needled Composite Laminates

5a. CONTRACT NUMBER

5b. GRANT NUMBER

5c. PROGRAM ELEMENT NUMBER

6. AUTHOR(S)
Ryan Emerson, Bradley Lawrence,[*] Andrew Montgomery,[†] and Sirina Safriet[‡]

5d. PROJECT NUMBER

5e. TASK NUMBER

5f. WORK UNIT NUMBER

7. PERFORMING ORGANIZATION NAME(S) AND ADDRESS(ES)
U.S. Army Research Laboratory
ATTN: RDRL-WMM-A
Aberdeen Proving Ground, MD 21005-5069

8. PERFORMING ORGANIZATION REPORT NUMBER
ARL-RP-472

9. SPONSORING/MONITORING AGENCY NAME(S) AND ADDRESS(ES)

10. SPONSOR/MONITOR'S ACRONYM(S)

11. SPONSOR/MONITOR'S REPORT NUMBER(S)

12. DISTRIBUTION/AVAILABILITY STATEMENT
Approved for public release; distribution is unlimited.

13. SUPPLEMENTARY NOTES
A reprint from the *Proceedings of the American Society for Composites 28th Technical Conference*, State College, PA, September 2013.
[*]Bowhead Science and Technology, Belcamp, MD
[†]Science and Mathematics Academy, Aberdeen, MD
[‡]Material and Manufacturing Directorate, Air Force Research Laboratory, Wright Patterson Air Force Base, OH

14. ABSTRACT
In the present investigation novel needle-processed S2-glass laminates are fabricated and several key failure modes are characterized. Double cantilever beam testing shows that mode I fracture toughness improves up to 270% compared to non-needled baseline material. In-plane compressive strength of needled material improves by up to 475%. In plane tensile strength shows mixed results, improving by 6% for moderate volume fractions of through-thickness reinforcement (TTR) and decreasing by 6% at larger volume fractions. Double lap shear tests show that interlaminar shear strength improves as much as 17% for TTR inserted at ±45° relative to the laminate plane. X-ray micro-computed tomography (micro-CT) is used to investigate the unique 3D microstructure resulting from the needling process for 90° TTR samples. The micro-CT reconstructions show that the dimensions of the disturbances of the inplane fabric are significantly smaller than those imparted by the conventional tufting or stitching processes at each penetration site. Micro-CT reveals that some penetration sites are aggregates of closely spaced neighbors, resulting from the lack of precise spatial control with the needling process used in the present research. At these aggregate locations the in-plane disturbances are roughly equal in size to those from tufting/stitching. Modifications to the automated processing equipment are shown and discussed. The modifications allow better spatial control at the penetration sites and the ability to insert TTR at ±45° relative to the laminate plane.

15. SUBJECT TERMS
composite, needling, characterization, processing, reinforcement, novel, interlaminar, TTR

16. SECURITY CLASSIFICATION OF:			17. LIMITATION OF ABSTRACT	18. NUMBER OF PAGES	19a. NAME OF RESPONSIBLE PERSON
a. REPORT	b. ABSTRACT	c. THIS PAGE			James Sands
Unclassified	Unclassified	Unclassified	UU	18	19b. TELEPHONE NUMBER (*Include area code*) 410-306-0403

Improvements to the Processing and Characterization of Needled Composite Laminates

R. EMERSON[1], B. LAWRENCE[2], A. MONTGOMERY[3] AND S. SAFRIET[4]

ABSTRACT

In the present investigation novel needle-processed S2-glass laminates are fabricated and several key failure modes are characterized. Double cantilever beam testing shows that mode I fracture toughness improves up to 270% compared to non-needled baseline material. In-plane compressive strength of needled material improves by up to 475%. In plane tensile strength shows mixed results, improving by 6% for moderate volume fractions of through-thickness reinforcement (TTR) and decreasing by 6% at larger volume fractions. Double lap shear tests show that interlaminar shear strength improves as much as 17% for TTR inserted at ±45° relative to the laminate plane.

X-ray micro-computed tomography (micro-CT) is used to investigate the unique 3D microstructure resulting from the needling process for 90° TTR samples. The micro-CT reconstructions show that the dimensions of the disturbances of the in-plane fabric are significantly smaller than those imparted by the conventional tufting or stitching processes at each penetration site. Micro-CT reveals that some penetration sites are aggregates of closely spaced neighbors, resulting from the lack of precise spatial control with the needling process used in the present research. At these aggregate locations the in-plane disturbances are roughly equal in size to those from tufting/stitching.

Modifications to the automated processing equipment are shown and discussed. The modifications allow better spatial control at the penetration sites and the ability to insert TTR at ±45° relative to the laminate plane.

[1]US Army Research Laboratory, RDRL-WMM-A, APG, MD.
[2]Bowhead Science and Technology, Belcamp, MD.
[3]Science and Mathematics Academy, Aberdeen, MD.
[4]Material and Manufacturing Directorate, Air Force Research Laboratory, WPAFB, OH

INTRODUCTION

Several approaches are described in the literature for improving the delamination resistance of composite materials through the use of so-called "3D" reinforcements, including Z-pins, stitches/tufts, knits and 3D weaves. The myriad of material combinations, applications/geometry and load spectra preclude conclusive statements on which of these is the best through-thickness reinforcement (TTR) technology but typically the benefits of 3D-reinforced composites carry tradeoffs in manufacturability, degradation of in-plane strength, and cost [1].

Another method for achieving a 3D architecture is needling (needle-punching). In this process, the 3D architecture is created with downward-barbed needles that push TTR into an otherwise 2D laminate. As such, needling is similar to stitching or tufting but with one important difference: the needling process typically inserts 20-60 through-thickness filaments at each penetration site, whereas the threads used in tufting and stitching are usually several thousands of filaments. This is significant because in-plane fiber distortion caused by the tuft/stitch thread is identified in the literature as the primary cause for the typical reported 5-15% reductions in the in-plane stiffness and strength [2,3]. Needled through-thickness reinforcement should thus incur less reduction in the in-plane strength because the fiber distortions are significantly reduced.

Needling was briefly evaluated as a 3D reinforcement method for structural composites under the Survivable, Affordable Reparable Airframe Program [4]. Several examples are found in the literature of needled/felted carbon-carbon (C/C) composites for high temperature applications such as ablative aerospace heat shields [5] and automobile brake pads [6]. The needled TTR in these previous reports was created by plunging downward-barbed needles through dry laminates of carbon fiber prior to pyrolisis, essentially breaking some of the in-plane carbon fiber to orient a fraction of the filaments in the through-thickness direction. The flexural strengths of the resultant needled C/C materials were reported in the range of 100-130 MPa and, as such, these materials are not relevant for high strength applications. Non-structural needled aramid fabric laminates are commercially available as air filtration media and in personnel protection products [7].

Proof-of-concept trials were recently conducted at the Army Research Laboratory (ARL) with dry plain-weave S2-glass laminate reinforced with aramid filaments in the through-thickness direction using a needling process and subsequently infused and cured with epoxy using vacuum-assisted resin transfer molding. The needling was performed using semi-automated processing equipment, commercial off-the-shelf (COTS) needles and COTS aramid mat designed for other applications. Needled material was tested under low velocity impact (LVI), compression after impact (CAI), in-plane compression and 4-pt bend. Needled specimens exhibited 10-15% increase in effective stiffness (force-deflection response) under LVI, 50% increase in CAI strength, 9% increase in in-plane compressive strength and 17% increase in flexural strength [8].

The literature provides no examples of the needling process and material as described in the present report. Figure 1 is an illustration showing the fundamental components and process of the present implementation of needling for structural applications. In this process, the downward-barbed needle picks-up and inserts so-called "supply" material into the 2-D laminate.

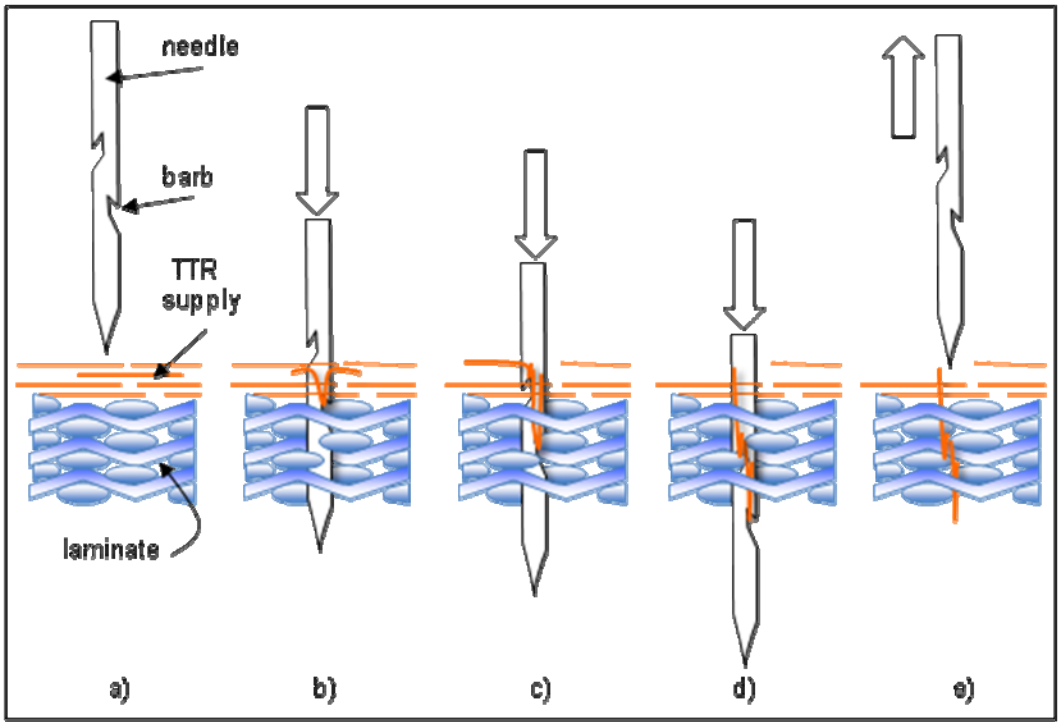

Figure 1. Illustration showing how the needle pushes supply material into the carrier material.

OBJECTIVE AND APPROACH

The objective of the present work is to extend the investigation of needling-processed material beyond the previous "proof-of-concept" experiments. Double cantilever beam (DCB) and double lap shear (DLS) tests are performed to assess improvements in mode-I fracture toughness and shear strength. Tension and compression tests are performed to assess the effects of needling on the in-plane mechanical behavior of the material. Micro-CT is used to gain insight to the microstructure resulting from the needling process.

EXPERIMENTAL

Materials

The in-plane reinforcement used for all specimens in the present investigation consists of cross-ply laminates of S2-glass plain weave fabric (813 g/m^2 per ply) [9]. Three plies of random-oriented aramid mat (34 g/m^2 per ply) with an epoxy-compatible sizing were used as the through-thickness reinforcement [10]. SC-15 toughened epoxy was used as the matrix for all specimens [11]. Thin (0.012 mm) ETFE film [12] was used as pre-crack material for the DCB specimens.

Needling

The needling facility is based on an *x*-*y* gantry custom-built at ARL with modular framing [13] and is shown in Figure 2. The gantry is clamped to a laboratory table and the facility is currently capable of processing flat plates of dimensions as large as 700 × 900 mm and up to 13 mm thick.

The two gantry axes move independently using stepper motors and a motion-control kit [14] that operates with G-code commands. These G-code commands are essentially a list of coordinates in *x*-*y* space to which the attached needling tool is driven at specific velocities. The hardware inside the needling tool converts the rotary motion of the motor to reciprocating motion (14.4 Hz) at the needles. The needles are held in three mounts and plunge through a hole in the "foot" of the tool as seen in Figure 3. All needles are shown installed in the mounts for illustrative purposes only – no samples were processed as part of this investigation with all needles installed. The stroke length of the 90° needles is 25.4 mm and the stroke length of the needles oriented at +45° and -45° are 35.9 mm. In this way, the *z*-component of the stroke of all needles is equivalent.

The height of the tool relative to the table surface is adjustable to accommodate different thicknesses of material. This adjustment includes springs that counteract most of the weight of the tool to prevent the tool from dragging material around the surface of the table. The height of the foot is also adjustable relative to the tool in order to control the depth of the needles into the material. The tabletop incorporates ten plies of 813 g/m^2 S2-glass weave covered with a 0.075 mm thick plastic sheet. This provides a firm backstop that is still permeable to the needles, allowing the TTR to be inserted completely through the laminate material during processing.

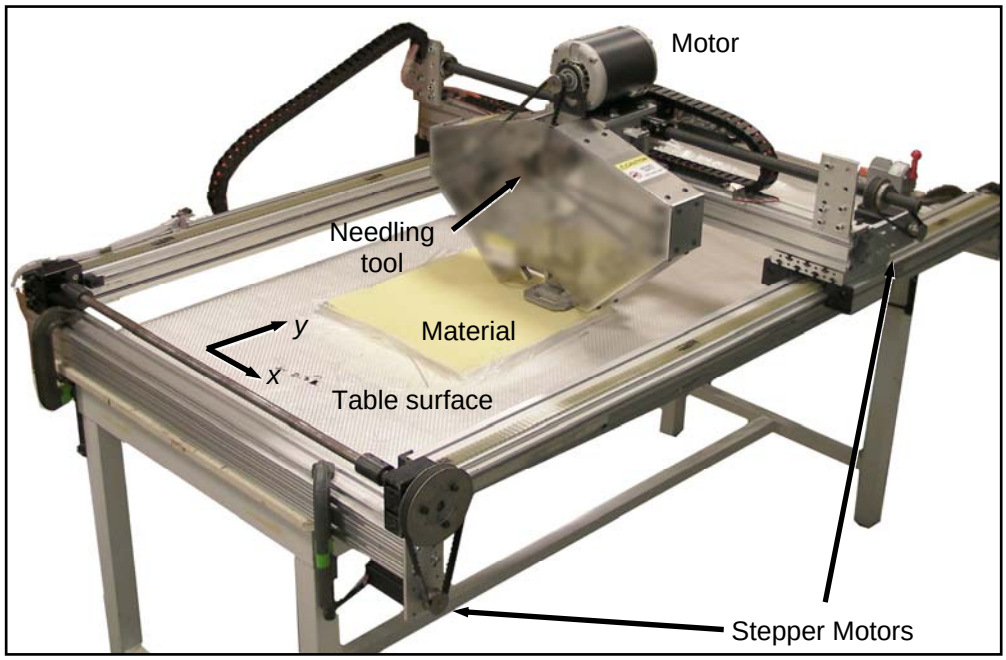

Figure 2. Photograph of the needling facility.

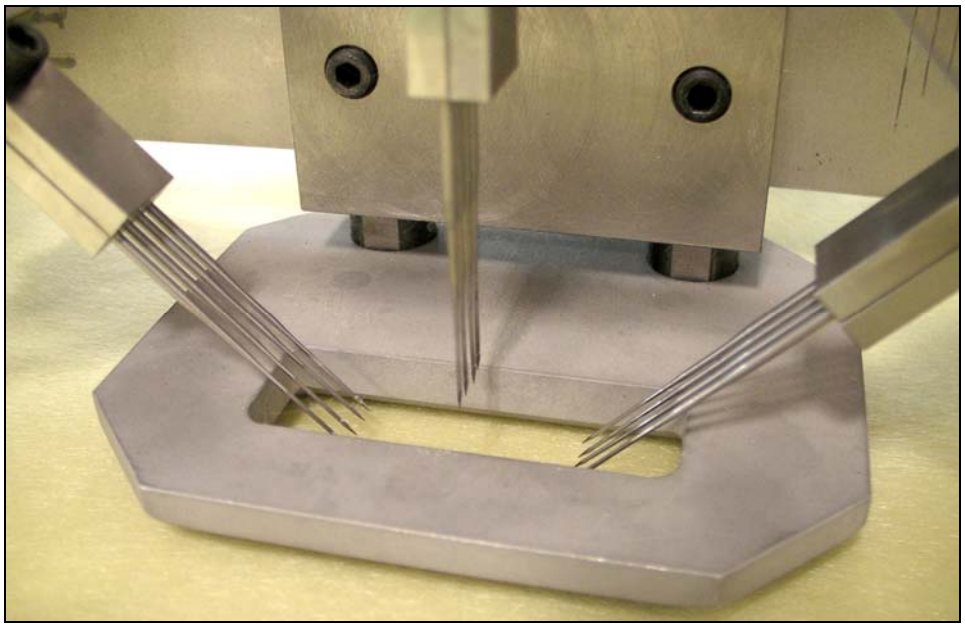

Figure 3. Needling foot with all needles installed.

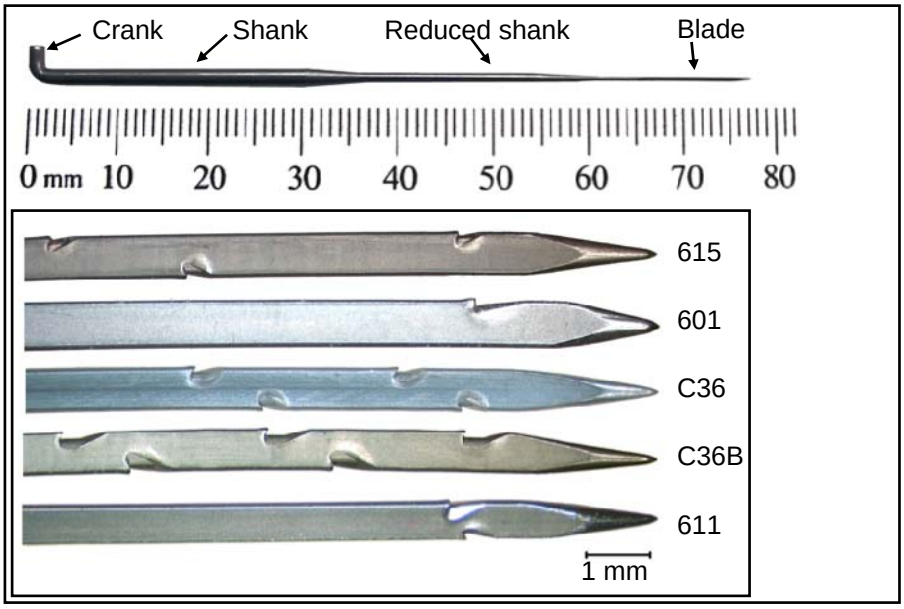

Figure 4. Labeled needle, inset shows close-ups of the blades of the different needles used in this investigation.

Figure 4 shows a labeled photograph of a typical needle. The inset in Figure 4 shows close-up images of the "blade" portions of the various needles used to make specimens for this investigation. The needled designated "601", "611", and "615" are products from Groz Beckert [15]. The "C36" and "C36B" needles are products from the Colonial Needle Company [16]. The cross-sections of all blades are

triangular, and there are barbs on the hidden apex of each needle with the exception of needle style 601 that only has a single barb on one apex.

Processing/Samples

For all test types, large "parent" panels were assembled on the needling table by first placing the S2 glass woven roving plies (813 g/m^2 per ply), then placing the aramid mat plies (34 g/m^2 per ply) on top. These dry stacks of material were then needle-processed in zones with different amounts of needling, henceforth referred to as "needling density" and expressed as penetrations per square cm (abbreviated p/cm^2). Figure 5 is an example illustration of the DCB parent panel, showing the zones of different needling densities. Note that control zones (i.e. zero p/cm^2) were included that incorporate the top plies of aramid mat but were not needled. All sample types came from panels that were needled in zones.

After the dry panels were needled they were transferred to a glass table and infused with epoxy using SCRIMP (Seeman Composites Resin Infusion Molding Process) then cured at 121°C in a convection oven. Post-cured specimens were then cut from the parent panels with a waterjet. Table I summarizes the relevant material details of the panels and specimens that were mechanically tested for this investigation.

Table I. PROCESSING DETAILS OF MATERIALS AND SPECIMENS

Specimen Type	S2 weave plies (*n*)	Aramid plies (*n*)	Needling Densities (p/cm^2)	Needle Type*	Specimen Size (L×W×t, mm)
DCB	10	3	0,12,24,47	C36	140×25×7.7
DLS	9	3	0,6,12,24	611	280×25×7.0
Tension	9	3	0,12,24,47	611	280×25×7.0
Com-pression	9	3	0,12,24,47	611	140×25×7.0
Micro-CT	11	3	6,12,24, 47,94	601, 615, C36B	10(diameter)×8.2

* Needle type shown in Figure 4

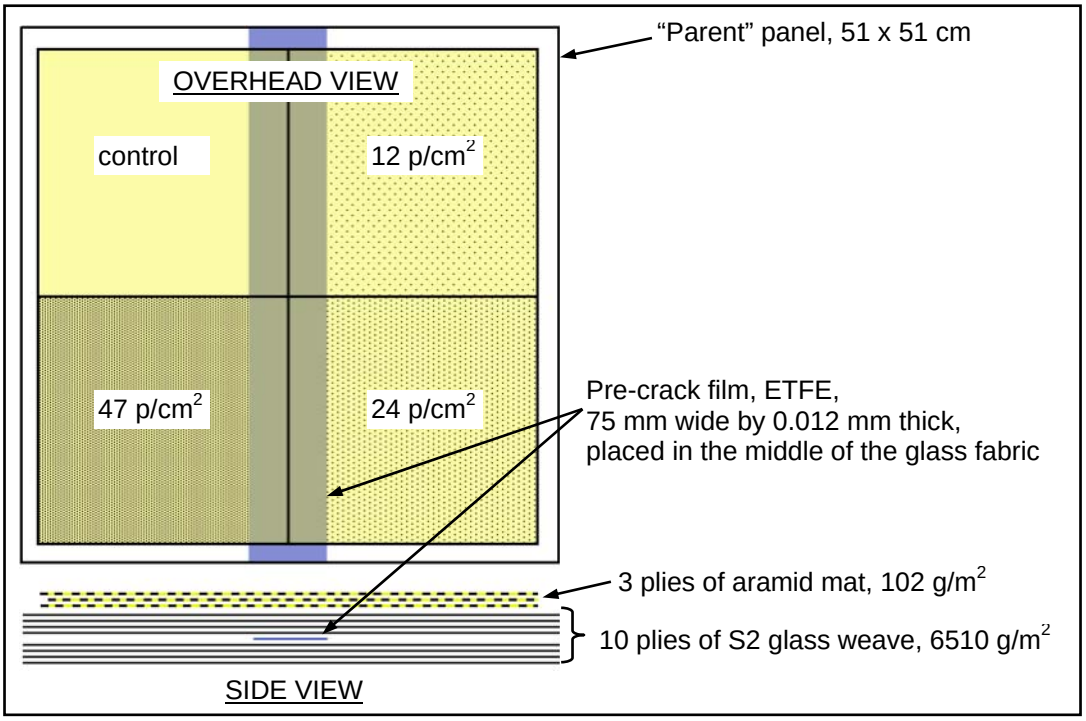

Figure 5. Illustration of processing zones for DCB parent panel.

Mechanical Testing

DCB specimens were prepared according to ASTM D5528-01 [17], with piano hinges bonded to the specimen arms using Hysol 9309 paste adhesive [18]. The DCB tests were conducted with an MTS Synergie 100 load frame [19]. Tension and compression testing was conducted with an Instron 1127 load frame [20] in accordance with ASTM D3039M-08 and ASTM D6641M-09, respectively [21-22]. Double lap shear tests were conducted with an Instron 4505.

Micro-CT and Optical Microscopy

Micro-CT was used to investigate the microstructure resulting from processing with different needling densities and needle types, and was not used post-mortem on any mechanical samples. Micro-CT was performed with an X-Tek HMX160 CT system [23]. The reflection X-ray tube uses a tungsten target with a focal spot of 5 μm and was set at 80 kV, 85 μA, no filtering. The composite specimens were adhered to the specimen holder using double sided tape and rotated over 360° in angular increments of 0.224° during each scan. Averages of four projection images (1024 x 1024 pixels) were collected at each position. X-ray images were reconstructed using CT Pro software version 2.0. Optical micrographs of the failure surface of a DCB specimen were captured using a Wild MZ3 optical microscope [24] with an integrated Diagnostic Instruments Insight 4 digital camera [25].

RESULTS/DISCUSSION

Mechanical Testing

Figure 6 shows the Mode-I delamination resistance curves for the DCB samples with fracture toughness G_I calculated using the modified beam theory method from [17],

$$G_I = \frac{3P\delta}{2ba}. \quad (1)$$

In this equation, P and δ are instantaneous crosshead load and displacement, respectively, b is sample width and a is the instantaneous crack length. Needling was observed to improve fracture toughness from the value of ~1750 J/m^2 measured on control material to ~6500 J/m^2 for material needled at 47 p/cm^2.

Figure 7 shows a comparison of the performance of DLS specimens processed with different needling densities. Data is presented as load frame force versus displacement and each data record is that of one representative specimen from a group of eight repetitions per condition. The inset in Figure 7 is a dimensioned side-view illustration of the DLS specimen showing the construction of the lap joint. Needling was used to reinforce the middle 152mm-long section of each specimen. All specimens failed in the desired shear mode at the lap joint. Compared to the control samples, needling at 90° and 45° only modestly increases the shear strength. A significant increase is observed in the initial slope of the force versus displacement response for specimens with 45° TTR.

Figure 8 shows the in-plane tensile and compressive strengths for different needling densities (all at 90°). Each column and error bar represents the average and standard deviation, respectively, for 8 repetitions per condition. Tensile strength is only slightly affected but compressive strength was observed to improve by up to 475% relative to the non-needled control material.

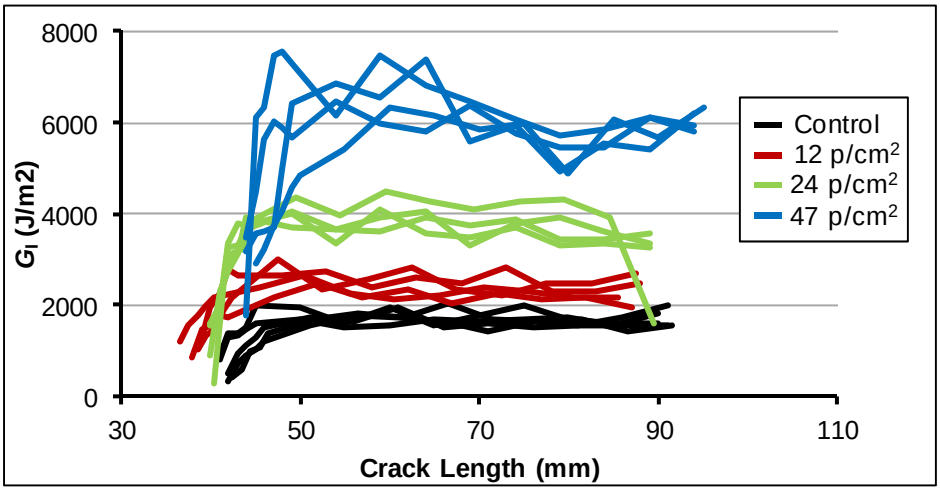

Figure 6. Delamination resistance curves for different needling densities.

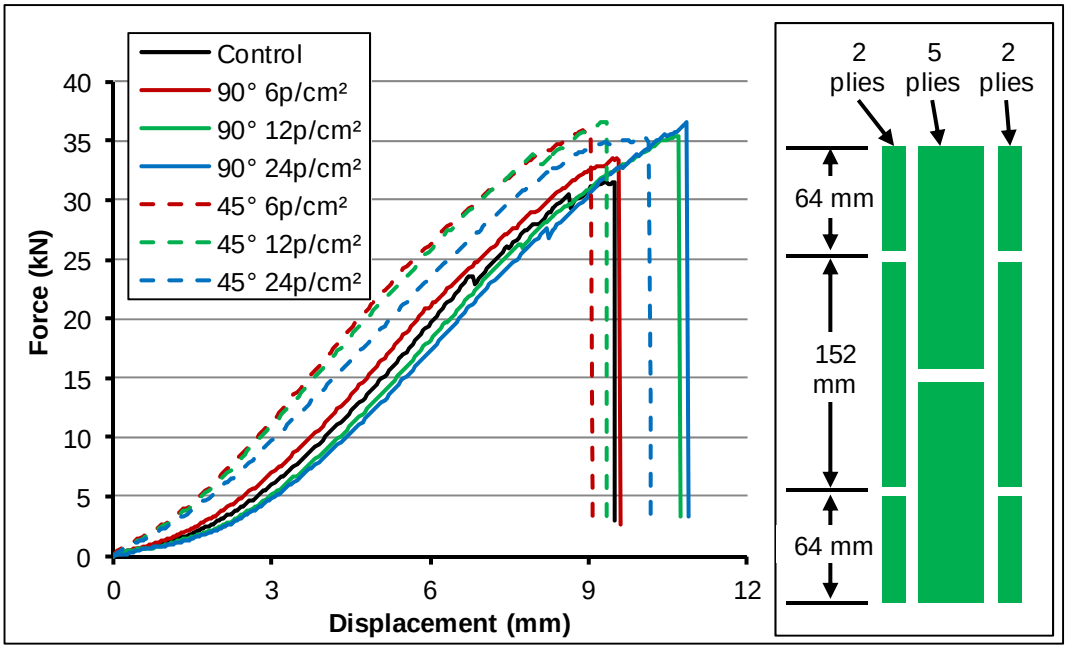

Figure 7. Comparison of performance of DLS specimens with different needling densities, inset shows specimen cross section.

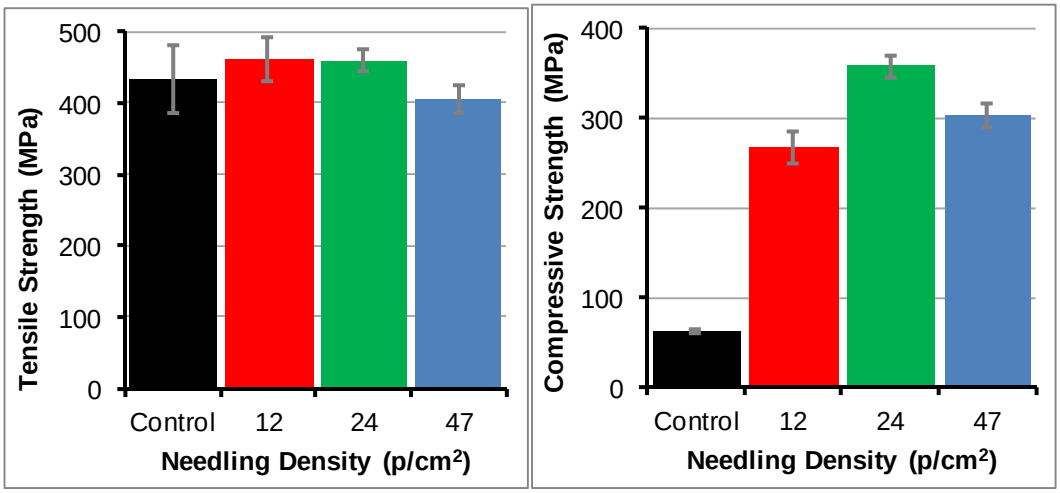

Figure 8. Tensile and compressive strength for different needling densities.

Micro-CT and Optical Microscopy

Figure 9 shows an example of top-view and side-view micro-CT images from a cylindrical specimen of material processed at 90° with a type 601 needle and 47 p/cm^2. The regions that are false-colored yellow (to improve visualization) correspond to the locations of aramid TTR and epoxy matrix because it was not possible to establish contrast between the two constituents. With micro-CT, it is possible to measure characteristic width of the TTR bundle at each penetration site for any given needle. For the type 601 and C36B needles with "aggressive" barbs, this width was observed to be 0.20-0.25mm wide per penetration. The width of the

TTR bundle from the less aggressive type 615 needle was less than 0.10 mm. These example micro-CT images also show that the TTR does not penetrate completely through the specimen thickness as a result of improper setting of the height of the foot on the needling tool. While not shown here in micro-CT images, the tool was set properly for the DCB, DLS, and tension and compression specimens as evidenced by visibly significant amounts of TTR pushed through the bottom of the panels.

Figure 10 shows an optical image of post-mortem fracture surface of a DCB specimen. The appearance of the TTR bundles protruding from the surface indicates that pull-out is a significant failure mode, although the appearance of curly-looking filament ends indicates that some amount of tensile failure in the TTR has occurred.

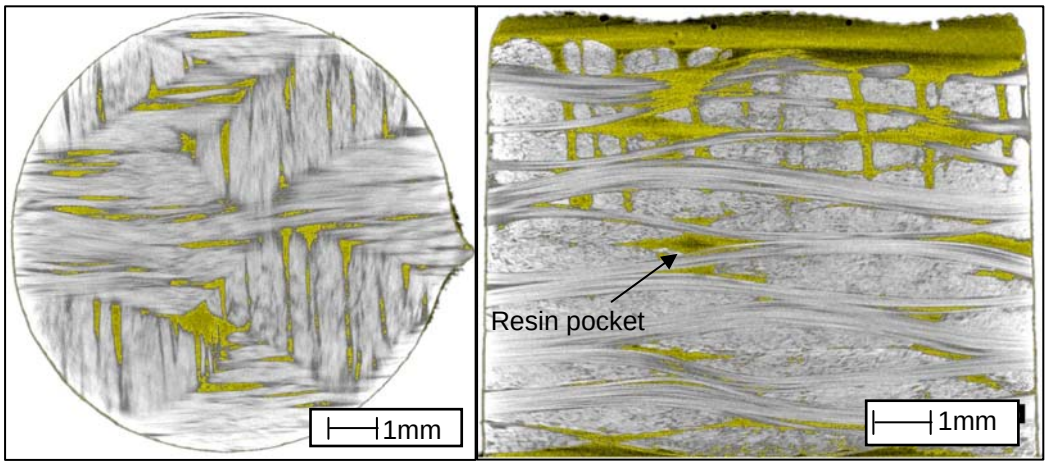

Figure 9. Top-view and side-view micro-CT images of material processed with a type 601 needle at 47 p/cm^2.

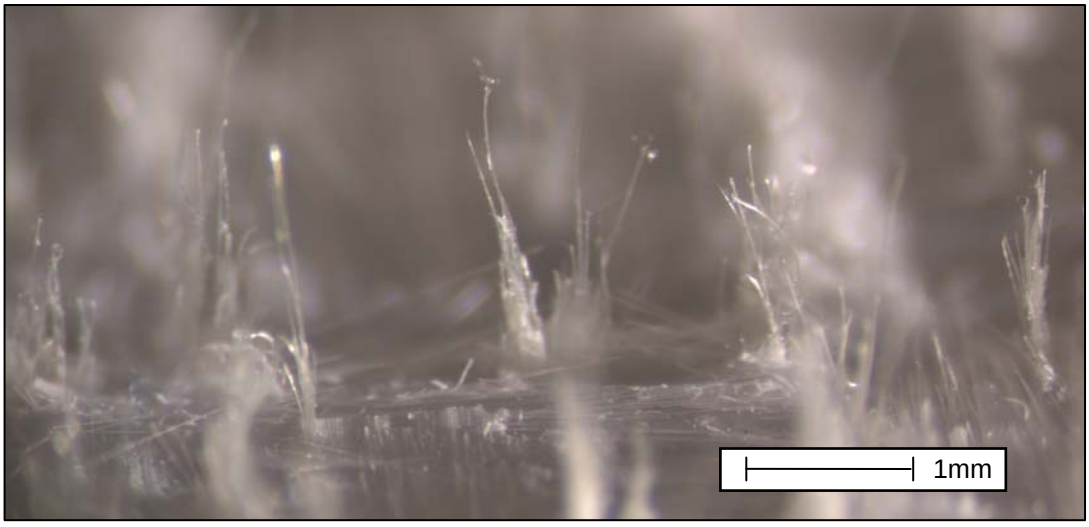

Figure 10. Optical image of post-mortem fracture surface of a DCB specimen.

CONCLUSIONS

The automated needling process described in the present report improved G_I and the in-plane compressive strength of woven glass laminates by 270% and 475%, respectively, without significantly degrading the in-plane tensile strength. The laminates with TTR oriented at 45° relative to the laminate normal exhibited only slightly improved shear behavior as measured with double lap shear tests.

Micro-CT was used to visualize the internal microstructure in needled material and to measure the width, penetration depth and distribution of the TTR bundles. Micro-CT will remain a useful tool during the continuing development of the needling process and needled composite materials.

REFERENCES

1. Mouritz, A.P., K.H. Leong and I. Herszberg. 1997. "A Review of the Effect of Stitching on the In-Plane Mechanical Properties of Fibre-Reinforced Polymer Composites" *Composites Part A*, 28A:979-991.
2. G. Dell'Anno, D.D. Cartié, I.K. Partridge, and A. Rezai. 2007. "Exploring Mechanical Property Balance in Tufted Carbon Fabric/Epoxy Composites," *Composites Part A*, 38:2366-2373.
3. De Verdiere, M.C., A.K. Pickett, A.A. Skordos, and V. Witzel. 2009. "Evaluation of the Mechanical and Damage Behaviour of Tufted Non Crimped Fabric Composites Using Full Field Measurements," *Composites Science and Technology*, 69:131-138.
4. Wilson, H., P. Minguet, J. Schaff, W. Townsend, and T. Davis. 2005. "Survivable, Affordable Reparable Airframe Program (SARAP) Technology Maturation and Trade Studies Structures Technology Final Report (Limited Distribution), *RDECOM TR06-D-10*.
5. Pierson, H.O. and D.A. Northrop. 1975. "Carbon-Felt, Carbon-Matrix Composites: Dependence of Thermal and Mechanical Properties on Fiber Precursor and Matrix Structure," *Journal of Composite Materials*, 9:118-137.
6. Han, C.-L., D.-L. Zhao, L. Zhang, and Z.-M. Shyen. 2010. "Microstructure and Mechanical Property of Three-Dimensional Needled C/SiC Composites Prepared by Precursor Pyrolysis," *Key Engineering Materials*, 434-435:45-47.
7. TexTech Industries, Portland, ME.
8. Emerson, R., J. Cain, M. Simeoni, and B. Lawrence. 2012. "Processing and Evaluation of 3D-Reinforced Needled Composite Laminate," *ARL-TR-6107*.
9. BGF Industries, Greensboro, NC.
10. Technical Fibre Products Inc., Schenectady, NY.
11. Applied Poleramic Inc., Benicia, CA.
12. Vac-Pac A6200, Cytec Industries, Inc. Woodland Park, NJ.
13. 80/20 Inc., Columbia City, IN.
14. http://www.automationtechnologiesinc.com/products-page/featured-cnc-products/g540-4-axis-nema23-381ozin-48v7-3a-psu Last accessed 5 June 2013.
15. Groz Beckert USA Inc., Charlotte, NC.
16. Colonial Needle Company, White Plains, NY.
17. ASTM D5528-01e3. 2007. "Standard Test Method for Mode I Interlaminar Fracture Toughness of Unidirectional Fiber-Reinforced Polymer Matrix Composites," ASTM International, West Conshohocken, PA.
18. Henkel Corporation, Madison Heights, MI.
19. MTS Systems Corporation, Eden Prarie, MN.
20. Instron, Norwood, MA.
21. ASTM D3039M-08. 2008. "Standard Test Method for Tensile Properties of Polymer Matrix Composite Materials," ASTM International, West Conshohocken, PA.
22. ASTM D6641M-09. 2009. "Standard Test Method for Compressive Properties of Polymer Matrix Composite Materials Using a Combined Loading Compression (CLC) Test Fixture," ASTM International, West Conshohocken, PA.

23. Nikon Metrology, Brighton, MI.
24. Wild Heerbrugg, Gais, Switzerland.
25. SPOT Imaging Solutions, Sterling Heights, MI.

NO. OF COPIES	ORGANIZATION
1 (PDF)	DEFENSE TECHNICAL INFORMATION CTR DTIC OCA
1 (PDF)	DIRECTOR US ARMY RESEARCH LAB IMAL HRA
1 (PDF)	DIRECTOR US ARMY RESEARCH LAB RDRL CIO LL
1 (PDF)	GOVT PRINTG OFC A MALHOTRA
1 (PDF)	RDRL WMM A B LAWRENCE

INTENTIONALLY LEFT BLANK.